Ecological Indicators 177 (2025) 113788

Contents lists available at ScienceDirect

Ecological Indicators

journal homepage: www.elsevier.com/locate/ecolind

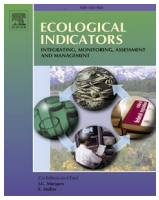

Original Articles

A novel framework for assessing shrublines and their geophysical constraints in alpine regions through probabilistic vegetation mapping and seed-filling algorithm

Zexi Ren [a,b], Lin Zhang [b,c,*], Qianlong Wang [d], Wanjun Hu [b,d], Zhou Shi [a,**]

[a] College of Environmental and Resource Sciences, Zhejiang University, Hangzhou 310058, China
[b] State Key Laboratory of Tibetan Plateau Earth System, Environment and Resources (TPESER), Institute of Tibetan Plateau Research, Chinese Academy of Sciences, Beijing 100101, China
[c] Key Laboratory of Biological Resources and Biosafety, Institute of Plateau Biology Research of Xizang Autonomous Region, Lhasa 850000, China
[d] School of Ecology and Environment, Tibet University, Lhasa 850000, China

ARTICLE INFO

Keywords:
Alpine shrublines
Geographical factors
Seed-filling algorithm
Woody vegetation classification
Vegetation index

ABSTRACT

Alpine shrublines are assumed to be highly sensitive to climate change and play a vital role in maintaining biodiversity and ecosystem functions. However, where and how alpine shrublines are distributed is poorly understood due to the difficulty in distinguishing between dwarf shrubs and grass. In this study, we proposed a novel framework to map alpine shrublines in Xizang Rezhen National Forest Park in 2020 using multi-source spatial data, probabilistic vegetation mapping, and seed-filling algorithm. Validation against high-resolution Google Earth imagery demonstrated a high accuracy, with a mean absolute error (MAE) of 5.2227 m and R^2 of 0.9935. The results indicated that the average elevation of alpine shrublines was about 4,899 m, ranging from 4,421 m to 5,163 m. South-facing alpine shrublines averaged approximately 101.7 m higher than north-facing counterparts. Meanwhile, shrublines at higher elevations exhibited lower EVI2 and NDVI values, suggesting reduced vegetation vigor under harsher environmental conditions. Among the environmental drivers, wind speed and minimum temperature were identified as key factors shaping the spatial patterns of shrubline elevation. Our findings offer insights into the current sensitivities and geographical influencing factors of the high-altitude woody ecosystems in this region, which are critical for understanding their potential ecological responses to climate change.

1. Introduction

Over recent decades, the Tibetan Plateau has experienced significant warming at a rate twice the global average, substantially impacting alpine vegetation dynamics (Chanda et al., 2024; Lu et al., 2020; Seastedt & Oldfather, 2021; Shangguan et al., 2024; Xu et al., 2024). Alpine shrublines that are transitional zones between woody and grassland ecosystems, represent the highest elevation and the low-temperature threshold at which woody vegetation can grow (Camarero et al., 2024; Lu et al., 2023). As such, they often serve as crucial conduits for species migration, facilitating the movement and dispersal of organisms across different kinds of ecosystem. Although similar to alpine treelines, alpine shrublines occur at higher elevations, indicating more severe environmental and climatic conditions (Bader et al., 2021; Holtmeier & Broll, 2005). Therefore, studying the spatial distribution of alpine shrublines not only provides a key window for understanding the growth mechanism of mountainous woody vegetation (Bayle et al., 2024), but also plays a vital role in maintaining biodiversity, regulating hydrological cycles, and carbon storage (Wu et al., 2024).

Research about spatial distribution patterns of alpine shrublines has achieved some advancement. Lu et al. (2019) recorded the world's highest alpine shrubline at 5,280 m above sea level on the western Tibetan Plateau. The southeastern Tibetan Plateau hosted willow shrublines (*Salix* spp.) at elevations spanning from 4,500 to 5,000 m (Wang et al., 2021). These studies have offered valuable insights into the

* Corresponding author at: State Key Laboratory of Tibetan Plateau Earth System, Environment and Resources (TPESER), Institute of Tibetan Plateau Research, Chinese Academy of Sciences, Beijing 100101, China.
** Corresponding author at: College of Environmental and Resource Sciences, Zhejiang University, Hangzhou 310058, China.
E-mail addresses: zhanglin@itpcas.ac.cn (L. Zhang), shizhou@zju.edu.cn (Z. Shi).

https://doi.org/10.1016/j.ecolind.2025.113788
Received 21 May 2025; Received in revised form 12 June 2025; Accepted 18 June 2025
Available online 23 June 2025

altitude ranges and spatial patterns of alpine shrublines on the Tibetan Plateau. However, the majority of existing research relies on traditional field surveys and is limited in spatial coverage, making it difficult to capture the spatial patterns of alpine shrubline distribution at larger scales, especially in remote and inaccessible alpine areas. In recent years, remote sensing technology has emerged as a powerful tool for studying alpine ecotones like treelines and grasslines due to its advantages of large coverage, high temporal resolution, and cost-effectiveness (Bian et al., 2025; Garbarino et al., 2023). Liu et al. (2024) developed a graph-cut-based method to map alpine grasslines across the Tibetan Plateau with high accuracy ($R^2 > 0.95$, RMSE < 30 m), and He et al. (2023) developed a Closed-Loop Mountain Treeline (CLMT) algorithm for the accurate treeline extraction ($R^2 = 0.92$, RMSE $= 25$ m). These studies provide a strong foundation for alpine shrubline mapping, combined multi-source spatial data, machine learning techniques, and edge extraction algorithms. However, distinguishing shrubs from herbaceous vegetation remains a significant challenge in alpine environments due to their similar spectral signatures and structural characteristics, particularly in medium-resolution satellite imagery. This spectral confusion often leads to misclassification, thereby limiting the effectiveness of remote sensing techniques in accurately delineating shrubline boundaries. To our knowledge, remote sensing-based image classification approaches have not yet been specifically applied to the detection and delineation of alpine shrublines.

Many studies related shrubs have focused on shrub encroachment in arid and semi-arid zones with low elevations (Li et al., 2023; Torres et al., 2024). Malapane et al. (2024) utilized Landsat TM and OLI satellite data, combined with a Random Forest (RF) classifier, to monitor woody vegetation encroachment in the Letaba River catchment from 1989 to 2019, achieving an overall classification accuracy ranging from 91.7 % to 95.5 %. However, alpine ecosystems lack sufficient knowledge about the spatial patterns of alpine shrublines. The special climatic and ecological conditions of alpine ecotones determine that it is uncertain whether the patterns observed in the arid zone are applicable to the alpine environment.

The Tibetan Plateau, characterized by its unique climatic conditions and tectonic uplift, provides good conditions for the formation and growth of distinct ecological boundaries, such as alpine shrublines (Lu et al., 2021). They are highly sensitive to climate change, thus offering valuable insights into the impacts of global warming on mountainous ecosystems. Xizang Rezhen National Forest Park, located in the southeastern Tibetan Plateau, is an ideal place to study alpine shrubs due to its relatively rich woody vegetation resources (Langzhen et al., 2022). Therefore, we took it as a representative area to delineate alpine shrublines. In this study, we used multi-source spatial data (Sentinel-2 reflectance, climate, soil, and topography) with a Random Forest (RF) classifier and seed-filling algorithm to: (1) develop an automated and novel framework for delineating alpine shrublines and analyze their spatial patterns; (2) reveal the influencing factors in shaping alpine shrublines in Xizang Rezhen National Forest Park. It can help improve our understanding of the impacts of climate change on alpine ecosystems and for supporting effective conservation and management strategies.

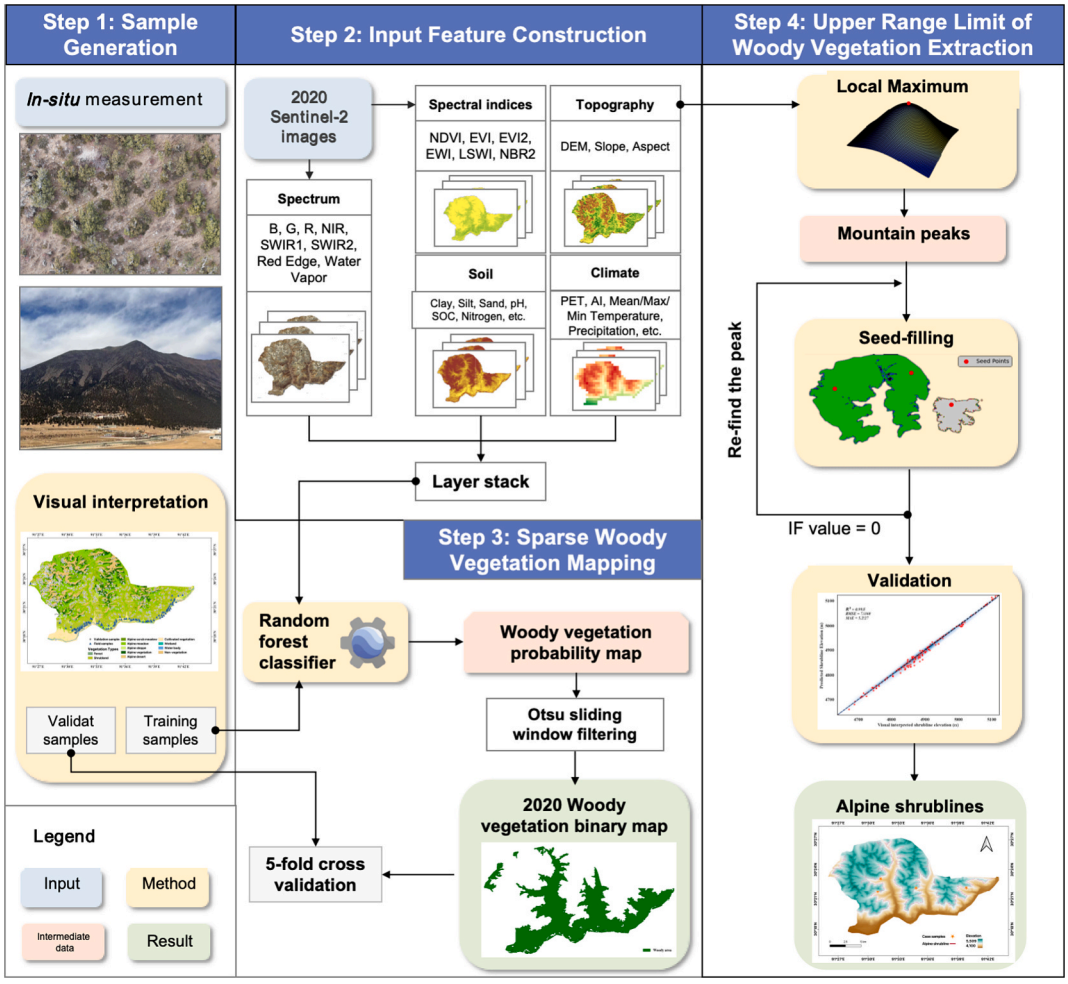

Fig. 1. Automated framework for alpine shrubline extraction and analysis.

2. Material and methods

This study developed a novel framework presented in Fig. 1 for delineating alpine shrublines comprising four key steps: sample point generation, multi-source data collection and preprocessing, woody vegetation binary map, and alpine shrubline extraction.

2.1. Study area

Xizang Rezhen National Forest Park (30°08'–30°27' N, 91°30'–91°42' E) (Fig. 2) is located in Linzhou County, Lhasa City, Xizang Autonomous Region, with an elevation ranging from approximately 4,200 to 5,500 m above sea level (Langzhen et al., 2022). It is characterized by a plateau temperate continental monsoon climate and distinguished by significant seasonal variability with long, cold, and dry winters, compared to short, warm, and humid summers. The mean annual temperature and precipitation during 1963–2020 at the nearest meteorological station in Dangxiong (30°28'N, 91°6'E; about 80,000 m west of the study area) was 2.1 °C and 475.2 mm, respectively. It is known for its unique ecological conditions and abundant biodiversity, especially the woody vegetation. There are about 220,000 ancient *Juniperus tibetica* trees, ranging in height from 3 to 12 m and age between 200 and 500 years, with some individuals potentially reaching a millennium in age (Li, 1993). In addition to the valuable *Juniperus tibetica* forests, the park maintains extensive and well-developed shrublands, covering large areas of the alpine zones and forming a distinct alpine ecotone between woody and herbaceous vegetation. Therefore, it serves as an ideal site for studying the spatial patterns of woody vegetation, particularly its upper limits. The main shrub species include *J. pingii* var. *wilsonii*, *Berberis hemsleyana*, etc.

2.2. Data

To accurately delineate alpine shrublines, it is essential to identify woody vegetation first. We selected multiple environmental variables, including topographic, soil, climatic, and spectral reflectance data derived from Sentinel-2 (Table S1) to identify pixels as woody vegetation. The elevation was derived from NASADEM_HGT dataset at a 30-meter spatial resolution (NASA JPL, 2020). Slope and aspect were calculated from the elevation data using the Google Earth Engine (GEE) platform. Soil content variables, including soil organic carbon (SOC), pH, clay, silt, sand, and bulk density (bdod), were derived from SoilGrids 2.0 at a 250-meter spatial resolution (Poggio et al., 2021), while daily soil moisture data at 1,000 m resolution were obtained from a China-specific dataset based on in-situ measurements (Shangguan et al., 2022). The climatic data were derived from Peng (2019) with a spatial resolution of 1, 000 m, and the bioclimatic variables were obtained from WorldClim version 2 (Fick & Hijmans, 2017) and listed in Table S2. Wind speed data (0.1° resolution) were provided by the National Cryosphere Desert Data Center (Zhang et al., 2021), and snow cover duration (500 m resolution) was sourced from a MODIS-based snow cover phenology dataset for China (Zhao et al., 2022). Here, all variables with a resolution coarser than 10 m were resampled to 10 m using bicubic interpolation in the GEE platform (Onačillová et al., 2022), which produces smoother gradients and edges compared to methods like nearest-neighbor or bilinear interpolation. Six popular auxiliary spectral variables (NDVI, EVI, EVI2, EWI, LSWI, NBR2, TWI, Li et al., 2022; Luo & Wu, 2022) and phenological parameters (EOS, SOS, LOS, Davison

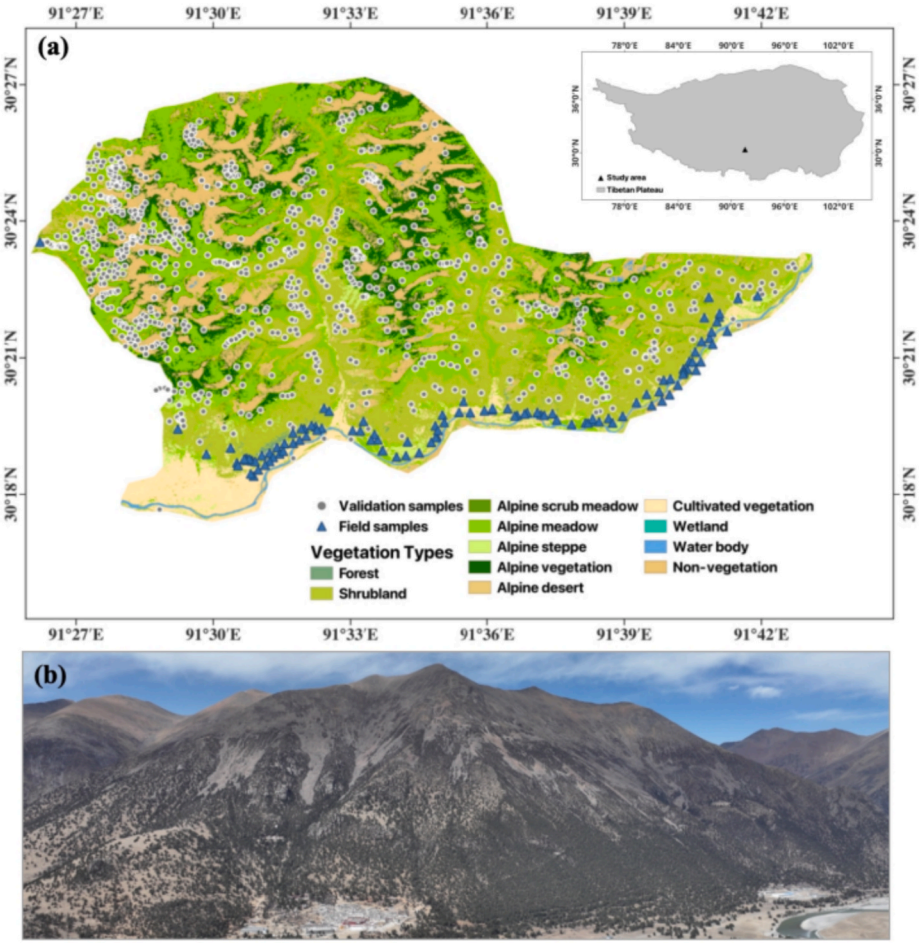

Fig. 2. The allocation and vegetation distribution of the Rezhen National Forest Park (a) and a UAV senary illustrating alpine shrublines (b).

et al., 2011; Didan, 2015) were derived from Sentinel-2 and MODIS data. The specific definitions of these indices are provided in Table S1.

2.3. Sparse woody vegetation classification method

Random Forest (RF), an ensemble learning method based on multiple decision trees, was employed to identify woody vegetation (Breiman, 2001). First, we utilized the "probability" mode of the RF in the GEE platform to generate a detailed probability map by calculating the probability of each pixel belonging to woody vegetation (Kruppa et al., 2014). The advantages of the probability map lie in their sensitivity to the continuous changes in vegetation along environmental gradients, with a quantifiable measure of confidence for the classification of each pixel. It is beneficial in ecological boundary extraction studies, where vegetation boundaries are generally discrete, thereby enhancing the accuracy and reliability of the classification results. We enhanced the accuracy and generalization capability of the model by implementing a 5-fold cross-validation strategy during training, where the predicted probabilities from each fold were averaged to generate the final probability map (Minowa, 2008). To convert the probability map into the woody vegetation binary map, we implemented an adaptive thresholding approach where the OTSU method was applied within sliding windows of varying sizes (initially testing from 10 × 10 pixels with 10-pixel increments) to determine the optimal window size, then iteratively traversing the entire image to enable localized optimal threshold determination at each window (Liu & Yu, 2009; Wang et al., 2023). Then, because woody vegetation classification results may still involve noise (e.g., salt-and-pepper effects), we applied morphological processing techniques to refine the results (Huang et al., 2009). We used a 3 × 3 pixel neighborhood for both erosion and dilation morphological filtering process, assisting in smoothing the boundaries and reducing noises in the predicted results. Finally, we applied a sieve filter method to remove isolated or fragmented woody vegetation pixels (Pereira et al., 2022).

2.4. Upper boundary extraction based on a seed-filling algorithm

To delineate the upper limits of alpine woody vegetation accurately, we implemented the top-down and seed-filling iterative algorithm. The algorithm initialized by extracting mountain peaks from a 30 m resolution DEM as seed points (He et al., 2023). Here, four mountain peaks were generated. Each peak started with an 8-neighbor search algorithm then moved down toward the valley. It expanded the connected region of the seed pixels based on neighborhood relationships, and redefined the connected region by removing the expanded pixels from the set until no further possible expansion. This process was repeated for each seed point until all points had been traversed. The boundaries of the labeled connected regions were then extracted using the "find_boundaries" function of the Python library scikit-image (Birinci & Kiranyaz, 2014). It was constrained to adjacency with woody vegetation pixels to filter out incorrect boundaries.

2.5. Validation

To achieve an accurate assessment of woody vegetation classification, we further validated the classification results by generating 200 random sampling points. The performance was evaluated using standard accuracy metrics derived from the confusion matrix (CM), including Overall Accuracy (OA), and the Kappa coefficient (Table 1). The identified alpine shrublines derived from the Sentinel-2 were validated against alpine shrublines visually interpreted using a combination of high-resolution Google Earth imagery and 3 m resolution PlanetScope imagery in the same period (2020), from which a sufficient number of validation points were randomly sampled. These points were then matched to the nearest pixels of the Sentinel-2-derived alpine shrublines based on the minimum distance matching method (Paulsen & Körner, 2014; Stueve et al., 2009). The accuracy was quantified using R^2 (Eq. (1)), Root Mean Square Error (RMSE) (Eq. (2)), and Mean Absolute Error (MAE) (Eq. (3)) metrics (Wei et al., 2020). Besides, we employed the VIEG model (Zou et al., 2023) to extract the average upper limit of woody vegetation in the study area as an independent validation of our results.

Table 1
Evaluation indicators of model performance.

Measure	Brief description	Equation
Overall Accuracy (OA) (Cai et al., 2021)	The overall predictive performance of the model	$\frac{1}{N}\sum_{i=1}^{n} x_{ii}$
Kappa (Cai et al., 2021)	The consistency between the forecast results and the true classification, which is used to measure the classification accuracy.	$\frac{\frac{1}{N}\sum_{i=1}^{n} x_{ii} - \sum_{i=1}^{n}(x_{i+}x_{+i})}{N^2 - \sum_{i=1}^{n}(x_{i+}x_{+i})}$

Note. N denotes the total number of samples; in the CM, n denotes the total number of classes, x_{i+} denotes the total number of rows, x_{+i} denotes the total number of columns, and x_{ii} denotes the number of correctly classified samples.

$$R^2 = 1 - \frac{\sum_{i=1}^{N}(y_i - \hat{y}_i)^2}{\sum_{i=1}^{N}(y_i - \bar{y})^2} \quad (1)$$

$$RMSE = \sqrt{\frac{1}{N}\sum_{i=1}^{N}(y_i - \hat{y}_i)^2} \quad (2)$$

$$MAE = \frac{1}{N}\sum_{i-1}^{N}|y_i - \hat{y}_i| \quad (3)$$

Here, $\hat{y}_i$ is the predicted shrubline elevation, y_i is the interpreted shrubline elevation, $\bar{y}$ is the average of the elevation of interpreted shrublines, and N is the total number of samples.

2.6. Statistic

Statistical analysis and data visualization were conducted using R (version 4.1.2) and Python (version 3.9). GEE was primarily used for data preprocessing and RF classification, while Python was employed for the binary classification, morphological operations, and the OTSU thresholding (Huang et al., 2009). Pearson's correlation coefficient was applied to analyze relationships between alpine shrubline elevation and environmental variables, with significance tested at $P < 0.05$ (Sedgwick, 2012). Graphical outputs, including frequency histograms and scatterplots, were generated using ggplot2 in R and Matplotlib in Python (Ostrowski & Menyhárt, 2020).

3. Results

3.1. Woody vegetation classification

Fig. 3(a) showed that the distribution of woody vegetation had obvious spatial heterogeneity, and the probability of coverage gradually decreased with increasing altitude. Specifically, darker green areas indicated areas with higher probability of woody vegetation cover, mainly at lower elevations. In the binary forest map, pixels with high probability of woody vegetation classification were extracted as the final woody vegetation coverage (Fig. 3b). The extracted woody vegetation in 2020 was about 1,467.74 ha, which was nearly 45 % of the total study area. Variable importance analysis (Fig. 3c) identified elevation as the strongest predictor (12.49), followed by Sentinel-2 bands B4 (11.53), B5 (10.86), and B3 (10.72). The enhanced vegetation index (EVI2, 8.88) and the minimum temperature of the coldest month (bio6, 7.09) were the most influential vegetation and climate predictors respectively, with precipitation (5.85) being among the top determinants of woody

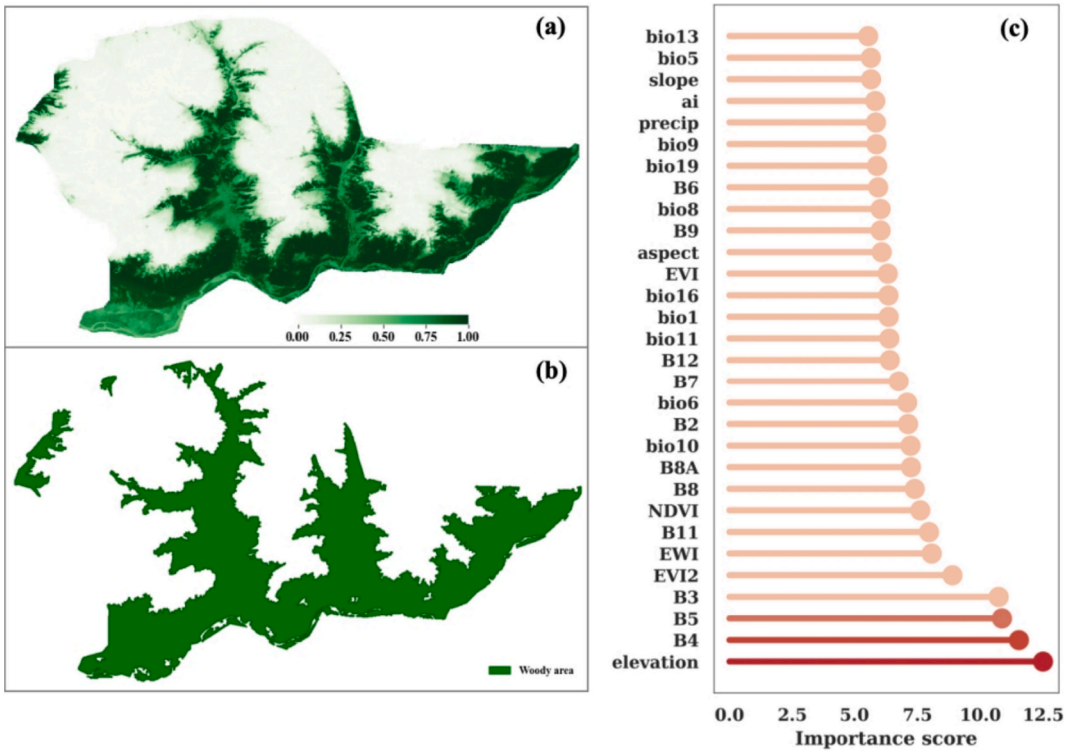

Fig. 3. (a) Probability and (b) binary map for woody vegetation in Xizang Rezhen National Forest Park. (c) Feature importance for classification.

vegetation distribution. As illustrated by Fig. 4(a), a 110 × 110 pixel window achieved optimal classification performance specifically for woody vegetation detection. This finding was validated through 5-fold cross-validation (Fig. 4b), with the mean overall accuracy of 0.9395 (± 0.0079) and Kappa coefficient of 0.8779 (± 0.0159).

3.2. Spatial distribution of the upper limits of shrubland

Fig. 5(a) showed substantial alignments between alpine shrubline distribution and elevation gradients, especially in areas with steep variations. The predicted alpine shrublines aligned well with observable landscape features in Google Earth imagery (Fig. 5b-e). Fig. 5(c) captured a landslide-induced downward shift in alpine shrublines. The predicted alpine shrubline elevations derived from Sentinel-2 closely matched visual interpretation shrublines derived from Google Earth image, with validation metrics of MAE = 5.2227 m, RMSE = 7.6360 m, and R^2 = 0.9935 (Fig. 5f). Sample comparisons of predicted versus visually interpreted shrubline elevations from PlanetScope (Fig. 5g) and Google Earth imagery (Fig. 5h) were provided, respectively.

3.3. Geographical characteristics of alpine shrublines

The elevation of the alpine shrublines ranged from 4,421 m to 5,163 m, with the average elevation of 4,899 ± 102 m (Fig. 6a). 80 % of the alpine shrubline elevation occurred between 4,773 m and 5,027 m. The alpine shrublines were mainly distributed in relatively steep areas with a slope of 20-40° and the average value of 31° (Fig. 6b). The spatial distribution of the alpine shrublines showed obvious direction dependency, with the frequency of distribution for south- (S) and southeast- (SE) facing being significantly higher than that of others (Fig. 6c). North-facing (N) and northwest-facing (NW) shrublines were less than 10 % of the study area's mean frequency, while those at the south-facing (S) direction accounted for the majority (>50 %) of observed shrubline distributions. As shown in Fig. 6(d), the distribution of the alpine shrublines at higher elevations was predominantly in the south direction, particularly above 4,800 m. Although the majority of alpine

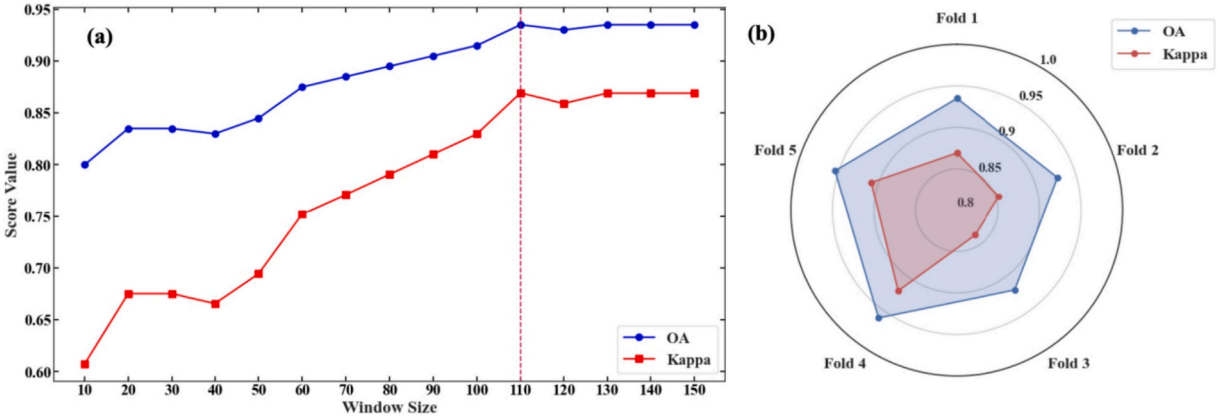

Fig. 4. (a) Accuracy and kappa scores across different window sizes; (b) Radar chart of OA and Kappa scores across 5-fold cross-validation.

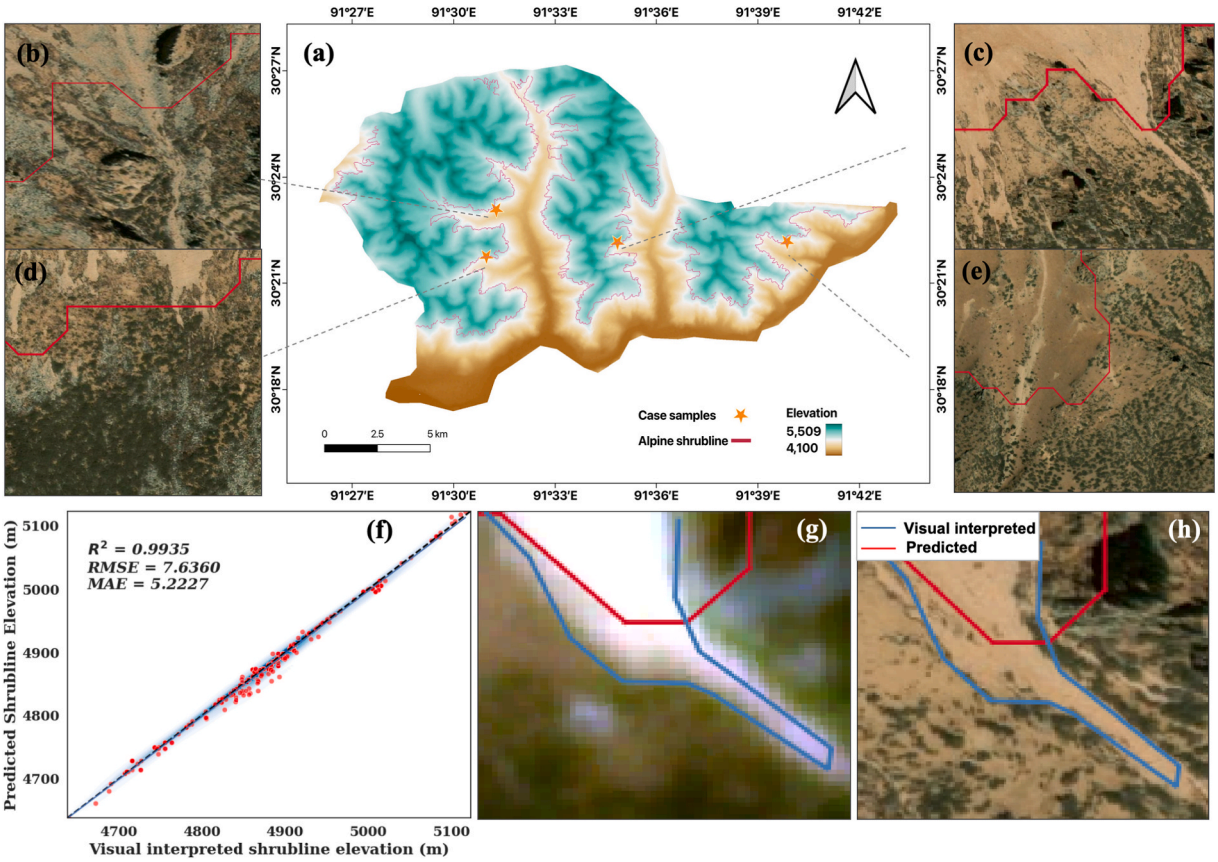

Fig. 5. The spatial distribution of shrublines (a) and typical cases (b-e) demonstrated in Google Earth, and scatter plot (f) with samples of predicted versus visual interpreted in PlanetScope (g) and Google Earth (h) shrubline elevation.

shrublines were on moderate slopes (20-40°), those at the N- facing showed a distinctive pattern of steeper slopes (30-40°) than gentle slopes (20-30°) (Fig. 6e). The mean NDVI value of the alpine shrublines was 0.21. The frequency distribution of NDVI was mainly between 0.1 and 0.4, with higher frequencies observed in the range of 0.2 to 0.3 (Fig. 6f). Compared to the NDVI values, EVI2 demonstrated a higher mean value of 0.55. The frequency distribution of EVI2 was primarily clustered between 0.2 and 0.8, with a notable peak in the range of 0.5 to 0.7 (Fig. 6g).

We constructed a relationship between the EVI2 and elevation in Fig. 7, displaying a notable turning point at an elevation of 4,750 m. Although this value is slightly lower than our predicted shrublines (4,899 ± 102 m), it remains broadly consistent with the elevation threshold distinguishing woody and herbaceous vegetation in the study area.

3.4. Correlation analysis of environmental variables with shrubline elevation

The two principal components (PC1 and PC2) accounted for 39.3 % and 23.5 % of the total variance, respectively (Fig. 8). The elevation was negatively correlated with PET (potential evapotranspiration), minimum temperature (tmn), and NDVI, as indicated by their vectors pointing in the opposite direction to that of elevation. In contrast, elevation exhibited a positive correlation with wind speed (WS) and snow cover duration (SCD), whose vectors aligned more closely with the direction of the elevation vector.

The shrubline elevation was significantly and positively correlated with wind speed ($r = 0.64$, $P < 0.001$, Fig. 9a). However, the minimum temperature was negatively correlated with the shrubline elevation ($r = -0.38$, $P < 0.001$, Fig. 9b). The shrubline elevation was also negatively correlated with PET ($r = -0.44$, $P < 0.001$, Fig. 9c). A weaker but still significant negative correlation was also observed with EVI2 ($r = -0.27$, $P < 0.001$; Fig. 9d).

4. Discussion

4.1. Comparison with other studies

Alpine shrublines exhibit considerable variation in relation to geographical location, prevailing microclimates, and the composition of the native species. For instance, shrubline elevations typically range from 1,600 to 2,500 m in the European Alps (Francon et al., 2021), but reach up to 4,000 m in the South American Andes (Hertel & Wesche, 2008). In Russia's Altai Mountains, the elevation of alpine shrublines is between 2,000 and 2,500 m because of the colder continental climate and reduced solar radiation (Tchebakova et al., 2009). Wang et al. (2021) reported that willow shrublines (*Salix* spp.) reaches 4,500–5,200 m on the southeastern Tibetan Plateau (approximately 29°–30°N), whereas the current highest alpine shrublines in the western Tibetan Plateau maintains an elevation of 5280 m (Lu et al., 2019). These findings, based on field sampling at similar latitudes, align closely with our results in Xizang Rezhen National Forest Park (30°8'N–30°27'N).

4.2. Topographic controls on alpine shrubline variation

The strong influence of elevation on the delineation of the alpine shrublines was obvious as shown in Fig. 5(a), because environmental factors such as temperature, moisture availability, and snow depth conditions vary systematically with altitudes. In steep regions, woody vegetation boundaries are sharper, marking the transition from favorable low-elevation locations to harsher conditions at high altitudes.

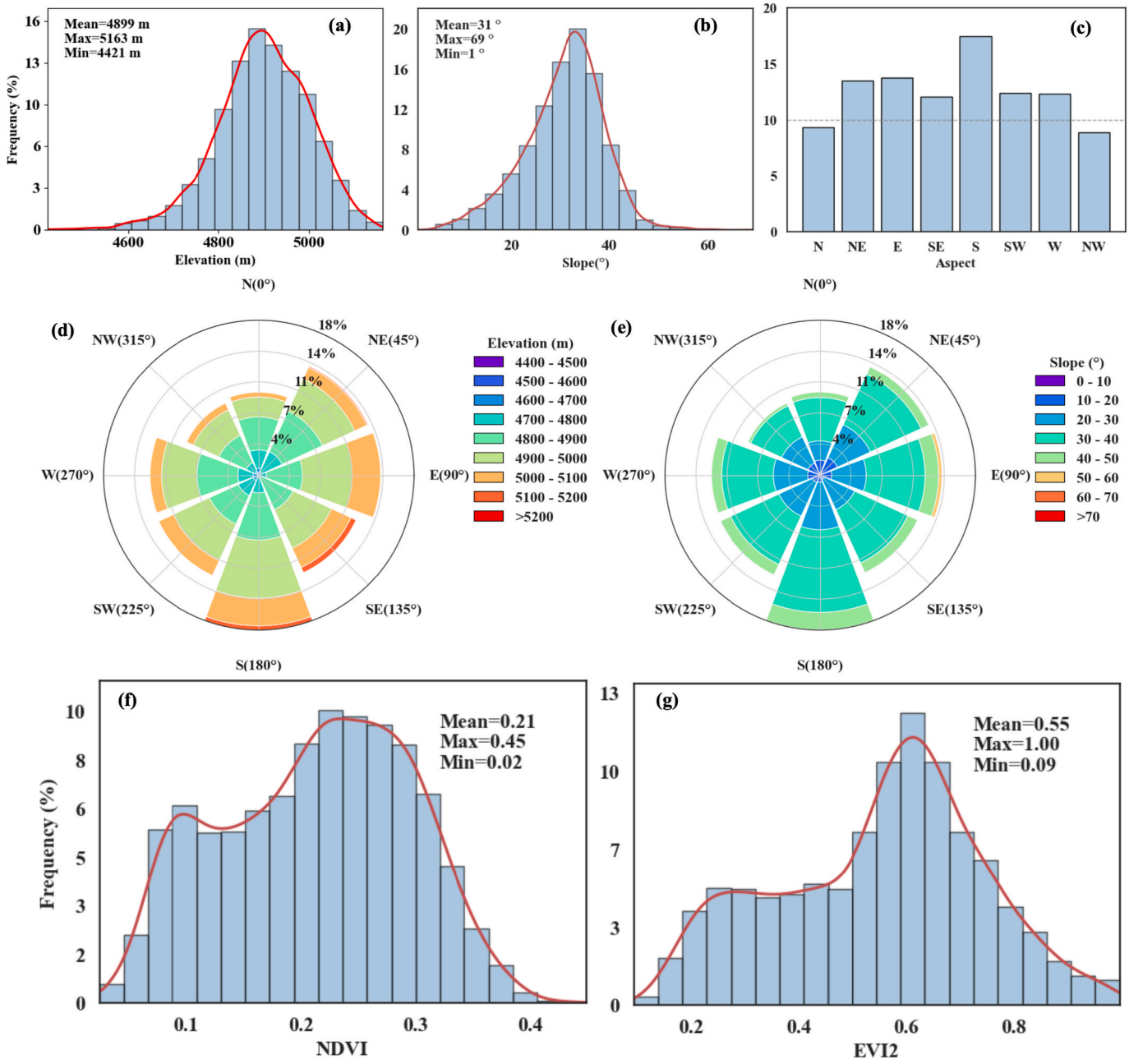

Fig. 6. Frequency histogram plots of terrain factors and vegetation spectral factors for shrublines in Xizang Rezhen National Forest Park. (a) Elevation, (b) Slope, (c) Aspect, (d) Synthesis of aspect and elevation, (e) Synthesis of aspect and slope, (f) NDVI, (g) EVI2.

Shrubline elevations in our study area correlate strongly with topographic factors such as slope (Fig. 6b) and aspect (Fig. 6c). Fig. 6(c) demonstrated that the majority of shrubline elevations on the N- and NW-facing directions were below 10 % compared to those observed on the S-facing, highlighting the pronounced effect of aspect on shrubland distribution. Our result found that the S-facing shrublines averaging approximately 101.7 m higher than the N-facing shrublines, where solar radiation was more intense, creating warmer and more favorable conditions for vegetation growth. This pattern aligns with global observations, where aspect plays a critical role in determining the distribution of alpine vegetation (Körner, 2007). Zhang et al. (2014) also found that the timberline elevation of *Juniperus saltuaria*-dominated forests on the S-facing direction (4,425 m) exceeds that of *Abies forrestii* var. *smithii* forests on the N-facing direction (4,320 m) by 105 m in the Sergymla Mountain of Southeast Xizang, due to increased solar radiation and relatively higher temperatures on the S-facing. The absence of alpine shrublines on the N-facing direction in Rezhen National Forest Park may be attributed not only to reduced solar radiation but also to their characteristically steeper gradients. As illustrated in Fig. 6(e), the N-facing shrublines were predominantly confined to slopes exceeding 30°, a topographic that may not be conducive to vegetation establishment owing to mechanical instability (Van Staden et al., 2021).

4.3. *Environmental interactions shape alpine shrubline patterns*

The correlation analysis of environmental variables with shrubline elevation revealed several key patterns of complex interactions between elevation, soil properties, climate, and vegetation health. Shrubline elevation showed a negative correlation with vegetation spectral indices such as EVI2 (Fig. 9d), indicating that vegetation at higher elevations

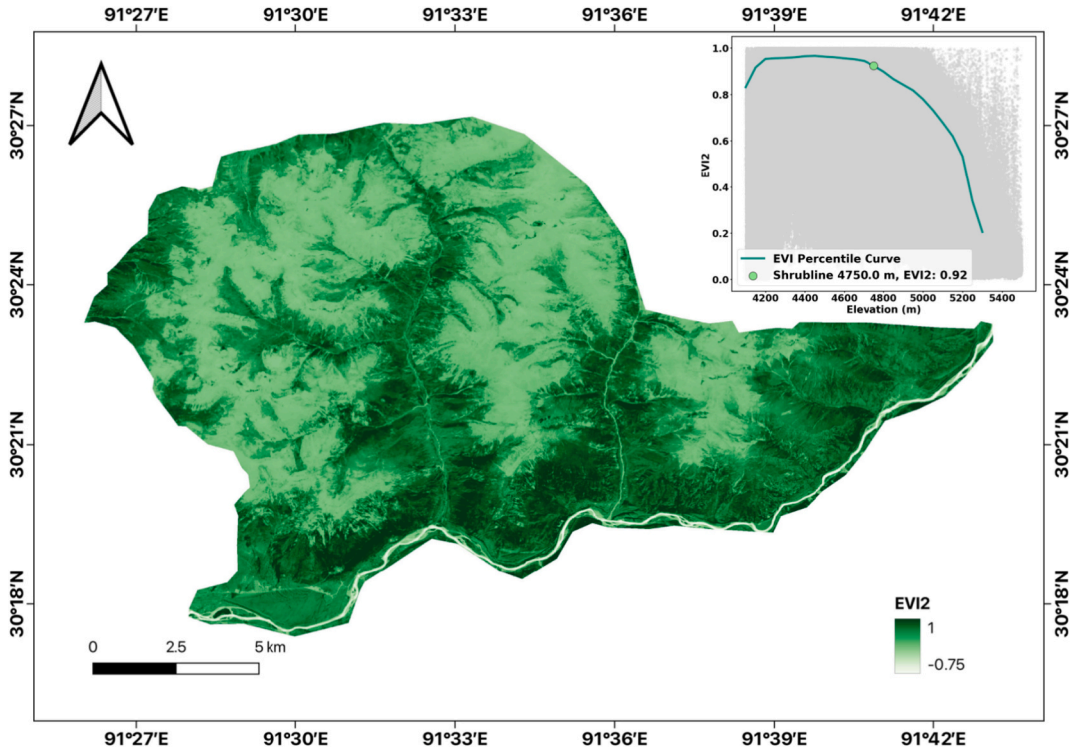

Fig. 7. Spatial distribution of EVI2 and its relationship with elevation.

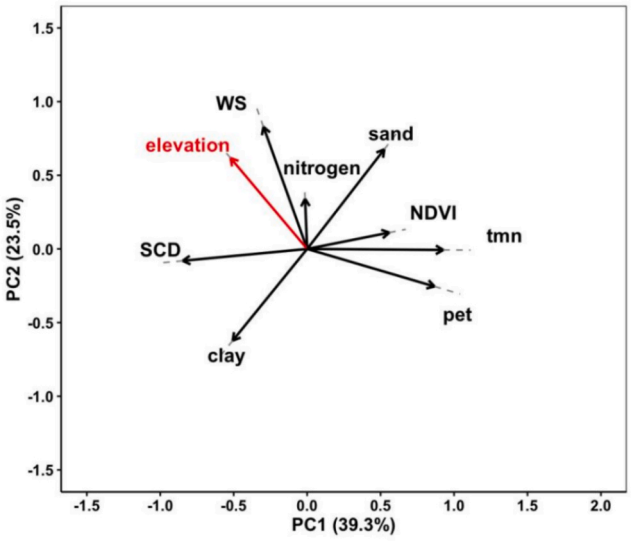

Fig. 8. PCA Biplot of environmental and vegetation variables for alpine shrublines in Rezhen National Forest Park.

tends to display reduced vigor and cover. This deterioration in vegetation condition may reflect the cumulative effects of environmental stressors, including cold temperatures, reduced moisture availability, and intensified wind exposure. This is further supported by the observation that shrubline elevation showed a strong positive correlation with wind speed (Fig. 9a), and negative correlations with minimum temperature (Fig. 9b) and PET (Fig. 9c). These climatic patterns suggest that shrubline position is primarily limited by colder and drier conditions at higher elevations, resulting in reduced energy and moisture availability for vegetation growth. Higher wind speeds at elevated areas may exacerbate water loss and cause physical damage to shrubs, limiting their growth. Wind-driven snow abrasion can suppress vertical shrub growth at high elevations (Brodersen et al., 2019), similar to its effect on timberlines. Strong winds also enhance evaporation, exacerbating drought stress and pushing shrubs toward their physiological limits (Paulsen & Körner, 2014).

Although the strength of the correlations varies, the overall weak associations suggest that these factors only explain a portion of the mechanisms influencing shrubline spatial patterns, and that shrubline formation is likely influenced by multiple unmeasured environmental drivers (Körner, 2003; Camarero et al., 2024). Among these, geomorphic disturbance plays a critical role, potentially limiting vegetation upslope expansion even under favorable climatic conditions. For example, Macias-Fauria & Johnson (2013) demonstrated that the upslope advance of subalpine forests induced by warming is significantly constrained by geomorphic processes. Smith et al. (2009) reported declines in chlorophyll content and photosynthetic efficiency at high elevations, while recent studies have emphasized the importance of drought stress and soil moisture limitations in restricting alpine plant growth (Zhang et al., 2024; Liang et al., 2024). These findings collectively indicate that the upper elevational limits of woody vegetation result from a complex interplay of climatic and physiological constraints. Furthermore, the coarse spatial resolution of climate data (approximately 1,000 m) may obscure fine-scale environmental heterogeneity in alpine terrain. Many datasets were originally generated at even coarser resolutions (1–10, 000 m) and resampled via smoothing or interpolation, which may further dampen local variability and reduce the strength of correlations. Future research should integrate higher-resolution and more spatially extensive datasets to better elucidate the complex ecological mechanisms underlying shrubline dynamics.

4.4. Uncertainties and perspectives

While predicted shrubline elevations aligned well with visual interpretations from high-resolution imagery (Fig. 5f), uncertainties remain due to limitations in multi-source data, algorithms, and the validation process itself. Obtaining accurate ground-truth data was challenging because alpine shrublines lie above 4,500 m and many sites

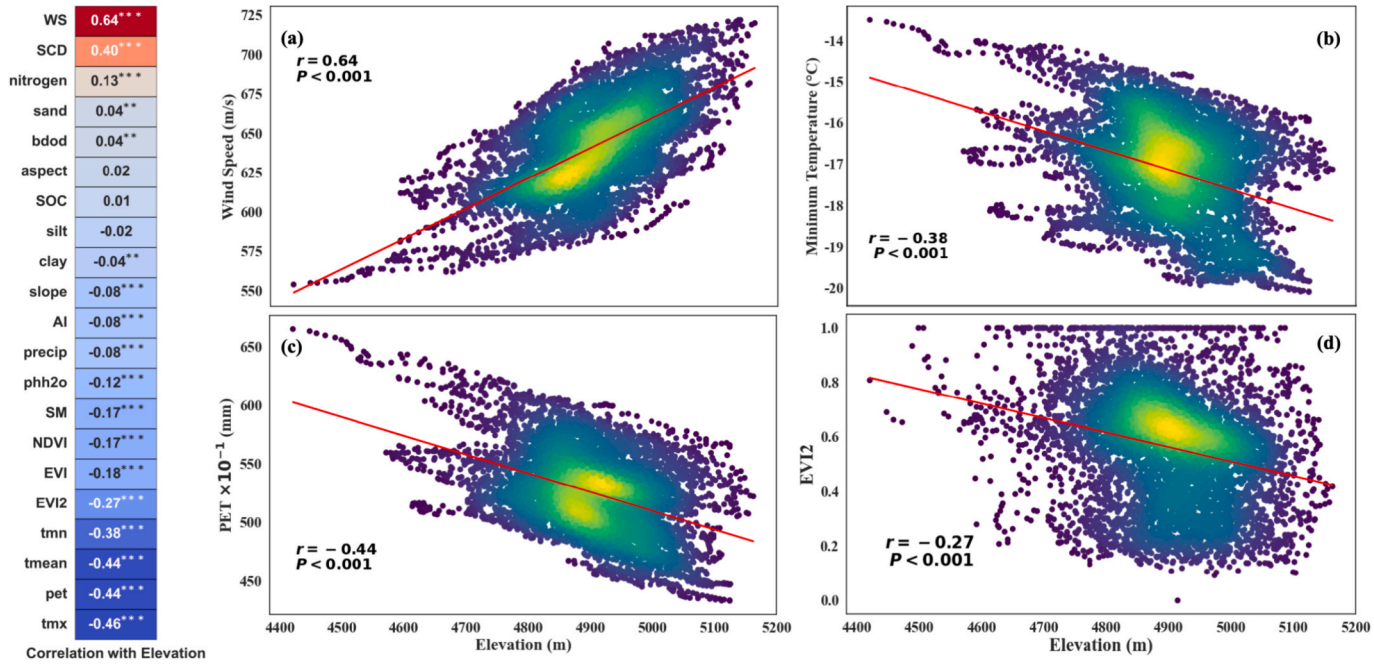

Fig. 9. Correlation between the elevation of the alpine shrublines and environmental variables for Xizang Rezhen National Forest Park. (a) Wind speed, (b) Minimum temperature, (c) PET, (d) EVI2.

are inaccessible by vehicle, making field validation unfeasible. Instead, we relied on visual interpretation using high-resolution Google Earth imagery and PlanetScope data as substitutes for ground-truth observations. While this approach provides a practical alternative due to access limitations, it may still introduce a degree of subjectivity. Future work could focus on field validations in more accessible shrubline regions, such as those at lower elevations or higher latitudes.

Another important source of uncertainty arises from the mismatch in spatial resolution between predictor and response variables (Garbarino et al., 2023). Environmental datasets, such as climatic variables from Peng (2019) at 1,000 m resolution and soil data from SoilGrids 2.0 at 250 m, were resampled to 10 m to align with the vegetation probability map. All data processing was performed on the GEE platform to ensure consistency and computational efficiency. Owing to the current limitations in GEE's resampling options (bilinear and bicubic interpolation), we adopted bicubic resampling, as it is generally more appropriate for continuous variables (Minh et al., 2024). However, this method introduces spatial averaging, potentially obscuring fine-scale environmental heterogeneity, particularly in complex alpine terrain where microclimatic variation is strongly shaped by topography and surface features. This smoothing effect may attenuate the observed correlations between environmental variables and shrubline elevation (Chen et al., 2023). For instance, the modest correlation (r = -0.38) between shrubline elevation and minimum temperature (Fig. 9b) may reflect the loss of local climatic variability during resampling. Such limitations likely contribute to underestimating the impact of environmental controls on the spatial distribution patterns of shrublines. Future studies should consider advanced downscaling techniques, such as dynamic downscaling, statistical disaggregation, or machine learning-based methods, which better preserve spatial heterogeneity and capture micro-scale ecological processes critical to alpine vegetation boundaries.

To overcome the uncertainty introduced by applying a global optimal threshold in the OTSU algorithm (Jian et al., 2025), we adopted a sliding window approach to determine locally optimal thresholds for binarizing the probability map. This method allows the threshold to adapt to spatial heterogeneity and reduces the risk of over- or under-classification in regions with varying environmental characteristics. However, there is still potential for further methodological improvements. For example, more advanced thresholding techniques, such as the three-dimensional OTSU algorithm, have proven effective in other remote sensing applications (Deng & Zhang, 2021), and may be explored in future work to further enhance classification accuracy in heterogeneous alpine environments. Although our alpine shrubline extraction framework effectively captured the overall spatial pattern of alpine woody vegetation, further improvements are needed to enhance accuracy and scalability. Future work should explore the integration of higher-resolution and structural remote sensing data to improve shrubline delineation, particularly in complex alpine environments. For example, incorporating canopy structural parameters from spaceborne LiDAR missions such as GEDI could provide valuable three-dimensional information for distinguishing shrub-dominated zones (Burns et al., 2024). Although Sentinel-2's 10 m spatial resolution is relatively high for large-scale vegetation mapping, it may still fail to capture fine-scale variations in shrubland distribution—particularly in sparsely vegetated or topographically complex areas—which can affect the accuracy of subsequent shrubline extraction. In contrast, PlanetScope imagery offers much finer spatial resolution, making it more suitable for detecting shrubline boundaries at local scales. However, its limited number of spectral bands constrains the amount of spectral information it can capture. Rösch et al. (2022) found that the overall classification accuracy of both datasets was comparable at broad scales, with Sentinel-2 being more efficient for large-area mapping. Nevertheless, the fine spatial detail of PlanetScope can complement the rich spectral information provided by Sentinel-2. Future studies may benefit from combining the strengths of both sensors to improve shrubline delineation in heterogeneous alpine landscapes.

In addition to these data considerations, the development of advanced algorithms, such as spectral mixture analysis, could further improve the detection of sparse and fragmented shrub vegetation (Yang et al., 2012). This approach would enhance shrubline delineation in areas where vegetation is less continuous, offering potential for future integration with our method. Our study area represents a typical alpine shrubland ecosystem on the Tibetan Plateau, providing meaningful insights into the spatial patterns of shrublines under high-altitude conditions. Nonetheless, to extend the applicability of these findings, future research should encompass broader regions such as the Himalayas and

other global alpine zones. Achieving this will likely depend on international collaboration to effectively validate and refine shrubline monitoring approaches across diverse mountain environments.

5. Conclusions

The results showed that the average elevation of alpine shrublines in Xizang Rezhen National Forest Park was 4,899 m, higher than that in other alpine systems (e.g., European Alps: 1,600–2,500 m; Andes: ≤4,000 m), reflecting the Tibetan Plateau's unique climatic-ecological conditions. The shrubline elevation is closely related to key climatic variables such as minimum temperature and wind speed. Previous alpine ecotone extraction methods have been limited in distinguishing woody from herbaceous vegetation due to their similar spectral features and structural properties. Our innovative framework overcomes these limitations by extracting precise alpine shrubline. Although this framework is innovative to some extent, there are still some uncertainties, particularly due to the spatial mismatch between high-resolution remote sensing data (10 m) and coarse environmental variables (e.g., 250 m soil and 1,000 m climate data), which may result in information loss during resampling. Additionally, unmeasured factors such as geomorphic disturbance may also influence shrubline patterns but are not captured by the current framework. Future research should consider incorporating higher-resolution environmental datasets and a broader range of ecological variables, along with advanced method to further improve the accuracy of shrubline extraction, contributing to more reliable monitoring and management of alpine ecosystems under global climate change.

Declaration of Generative AI and AI-assisted technologies in the writing process

During the preparation of this work the author(s) used DeepSeek in order to improve language clarity and correct grammatical errors. After using this tool/service, the author(s) reviewed and edited the content as needed and take(s) full responsibility for the content of the publication.

CRediT authorship contribution statement

Zexi Ren: Writing – original draft, Software, Methodology, Conceptualization. **Lin Zhang:** Writing – review & editing, Supervision. **Qianlong Wang:** Investigation, Data curation. **Wanjun Hu:** Investigation. **Zhou Shi:** Writing – review & editing, Supervision.

Declaration of competing interest

The authors declare that they have no known competing financial interests or personal relationships that could have appeared to influence the work reported in this paper.

Acknowledgments

This work was supported by the National Natural Science Foundation of China [Grant No. 32241036], and by the Science and Technology Projects of the Xizang Autonomous Region [Grant Nos. XZ202401JD0025 and XZ202501ZR0070]. We are grateful to Dr. Songchao Chen and Dr. Yihang Zhang for their valuable suggestions and insightful comments, which significantly improved the quality of this manuscript. We also sincerely appreciate the constructive feedback from the anonymous reviewers, whose thoughtful comments helped strengthen this work.

Appendix A. Supplementary data

Supplementary data to this article can be found online at https://doi.org/10.1016/j.ecolind.2025.113788.

Data availability

Data will be made available on request.

References

Bader, M.Y., Llambí, L.D., Case, B.S., Buckley, H.L., Toivonen, J.M., Camarero, J.J., Cairns, D.M., Brown, C.D., Wiegand, T., Resler, L.M., 2021. A global framework for linking alpine-treeline ecotone patterns to underlying processes. Ecography 44 (2), 265–292. https://doi.org/10.1111/ecog.05285.

Bayle, A., Carlson, B.Z., Nicoud, B., Francon, L., Corona, C., Lavorel, S., Choler, P., 2024. Uncovering the distribution and limiting factors of ericaceae-dominated shrublands in the french alps. Front. Biogeogr. 16 (1). https://doi.org/10.21425/F5FBG61746.

Bian, J., Li, A., Nan, X., Zhang, Z., Lei, G., Zhao, J., Naboureh, A., 2025. Stereoscopic remote sensing observation for mountains: advancing monitoring, modeling, and management. The Innovation 100838. https://doi.org/10.1016/j.xinn.2025.100838.

Birinci, M., Kiranyaz, S., 2014. A perceptual scheme for fully automatic video shot boundary detection. Signal Process. Image Commun 29 (3), 410–423. https://doi.org/10.1016/j.image.2013.12.003.

Breiman, L., 2001. Random forests. Mach. Learn. 45 (1), 5–32. https://doi.org/10.1016/j.image.2013.12.003.

Brodersen, C.R., Germino, M.J., Johnson, D.M., Reinhardt, K., Smith, W.K., Resler, L.M., Wieser, G., 2019. Seedling survival at timberline is critical to conifer mountain forest elevation and extent. Front. For. Global Change 2, 9. https://doi.org/10.3389/ffgc.2019.00009.

Burns, P., Hakkenberg, C.R., Goetz, S.J., 2024. Multi-resolution gridded maps of vegetation structure from GEDI. Sci. Data 11 (1), 881. https://doi.org/10.1038/s41597-024-03668-4.

Cai, W., Wei, Z., Liu, R., Zhuang, Y., Wang, Y., Ning, X., 2021. Remote sensing image recognition based on multi-attention residual fusion networks. ASP Trans. Pattern Recog. Intell. Syst. 1 (1), 1–8. https://doi.org/10.52810/TPRIS.2021.100005.

Camarero, J.J., Gazol, A., Tamudo, E., Moiseev, P.A., Colangelo, M., Valeriano, C., 2024. Local and regional climatic constraints of shrub and tree growth near the treeline. Dendrochronologia 88, 126256. https://doi.org/10.1016/j.dendro.2024.126256.

Chanda, R., Singh, S.S., Singh, N.S., Upadhyay, K.K., Tripathi, S.K., 2024. Two-decadal climate impacts on growth of major forest types of Eastern Himalaya. Trees, Forests and People 15, 100491. https://doi.org/10.1016/j.tfp.2023.100491.

Chen, J., Chen, Z., Huang, R., You, H., Han, X., Yue, T., Zhou, G., 2023. The effects of spatial resolution and resampling on the classification accuracy of wetland vegetation species and ground objects: a study based on high spatial resolution UAV images. Drones 7 (1), 61. https://doi.org/10.3390/drones7010061.

Davison, J.E., Breshears, D.D., Van Leeuwen, W.J., Casady, G.M., 2011. Remotely sensed vegetation phenology and productivity along a climatic gradient: on the value of incorporating the dimension of woody plant cover. Glob. Ecol. Biogeogr. 20 (1), 101–113. https://doi.org/10.1111/j.1466-8238.2010.00571.x.

Deng, Z., Zhang, G., 2021. An improved forest fire monitoring algorithm with three-dimensional Otsu. IEEE Access 9, 118367–118378. https://doi.org/10.1109/ACCESS.2021.3105382.

Didan, K., 2015. MOD13Q1 MODIS/Terra Vegetation Indices 16-Day L3 Global 250m SIN Grid V006. NASA EOSDIS Land Processes Distributed Active Archive Center. Accessed 2025-05-03 from https://doi.org/10.5067/MODIS/MOD13Q1.006.

Francon, L., Corona, C., Till-Bottraud, I., Choler, P., Roussel, E., Carlson, B.Z., Morin, S., Girard, B., Stoffel, M., 2021. Shrub growth in the alps diverges from air temperature since the 1990s. Environ. Res. Lett. 16 (7), 74026. https://doi.org/10.1088/1748-9326/ac0b67.

Fick, S.E., Hijmans, R.J., 2017. WorldClim 2: new 1-km spatial resolution climate surfaces for global land areas. Int. J. Climatol. 37 (12), 4302–4315. https://doi.org/10.1002/joc.5086.

Garbarino, M., Morresi, D., Anselmetto, N., Weisberg, P.J., 2023. Treeline remote sensing: from tracking treeline shifts to multi-dimensional monitoring of ecotonal change. Remote Sens. Ecol. Conserv. 9 (6), 729–742. https://doi.org/10.1002/rse2.351.

He, X., Jiang, X., Spracklen, D.V., Holden, J., Liang, E., Liu, H., Xu, C., Du, J., Zhu, K., Elsen, P.R., Zeng, Z., 2023. Global distribution and climatic controls of natural mountain treelines. Glob. Chang. Biol. 29 (24), 7001–7011. https://doi.org/10.1111/gcb.16885.

Hertel, D., Wesche, K., 2008. Tropical moist polylepis stands at the treeline in east Bolivia: the effect of elevation on stand microclimate, above- and below-ground structure, and regeneration. Trees 22 (3), 303–315. https://doi.org/10.1007/s00468-007-0185-4.

Holtmeier, F.K., Broll, G., 2005. Sensitivity and response of northern hemisphere altitudinal and polar treelines to environmental change at landscape and local scales. Glob. Ecol. Biogeogr. 14, 395–410. https://doi.org/10.1111/j.1466-822X.2005.00168.x.

Huang, X., Zhang, L., Wang, L., 2009. Evaluation of morphological texture features for mangrove forest mapping and species discrimination using multispectral IKONOS imagery. IEEE Geosci. Remote Sens. Lett. 6 (3), 393–397. https://doi.org/10.1109/LGRS.2009.2014398.

Jian, Z., Ai, B., Zeng, J., Sun, Y., 2025. A hybrid mangrove identification method by combining the time-frequency threshold of the mangrove index with a random forest binary classifier. IEEE J. Sel. Top. Appl. Earth Obs. Remote Sens. 18, 2077–2092. https://doi.org/10.1109/JSTARS.2024.3494058.

Körner, C., 2003. Alpine plant life. Springer. https://doi.org/10.1007/978-3-030-59538-8.
Körner, C., 2007. Climatic treelines: Conventions, global patterns, causes (klimatische baumgrenzen: konventionen, globale muster, ursachen). Erdkunde 61 (4), 316–324. https://www.jstor.org/stable/25648043.
Kruppa, J., Liu, Y., Biau, G., Kohler, M., König, I.R., Malley, J.D., Ziegler, A., 2014. Probability estimation with machine learning methods for dichotomous and multicategory outcome: Theory. Biom. J. 56 (4), 534–563. https://doi.org/10.1002/bimj.201300068.
Langzhen, J.Y., Zhang, Q.B., Jia, H., Zheng, J., Fang, J., 2022. Tree rings reveal a growth-decline event in AD 1875–1883 in a Tibetan plateau juniper forest. Dendrochronologia 74, 125981. https://doi.org/10.1016/j.dendro.2022.125981.
Li, B., 1993. The alpine timberline of Tibet. *In: Forest development in cold climates*. Springer US, Boston, MA, *pp. 511-527*. https://doi.org/10.1007/978-1-4899-1600-6_34.
Li, D., Liu, Y., Yang, X., Zhang, X., Shi, Z., 2023. Shrub encroachment alters plant trait response to nitrogen addition in a semi-arid grassland. Front. Plant Sci. 14. https://doi.org/10.3389/fpls.2023.1103371.
Li, X., Li, Y., Di, S., Niu, Y., Zhang, C., 2022. Evapotranspiration and land surface temperature of typical urban green spaces in a semi-humid region: Implications for green management. Front. Environ. Sci. 10, 977084. https://doi.org/10.3389/fenvs.2022.977084.
Liang, S., Liang, L., Wang, D., et al., 2024. Dryland Forestation in Focus: uncovering the carbon sequestration potential. Innovation Geosci. 2 (1), 100058. https://doi.org/10.59717/j.xinn-geo.2024.100058.
Liu, D., Yu, J., 2009. Otsu method and K-means. *2009 Ninth International Conference on Hybrid Intelligent Systems*, 1, 344–349. https://doi.org/10.1109/HIS.2009.74.
Liu, L., Chen, J., Shen, M., Chen, X., Cao, R., Cao, X., Cui, X., Yang, W., Zhu, X., Li, L., Tang, Y., 2024. A remote sensing method for mapping alpine grasslines based on graph-cut. *Gloabal Change*. Biology 30 (1). https://doi.org/10.1111/gcb.17005.
Lu, X., Hu, F., Liang, E., Sigdel, S.R., Shang, Z., Camarero, J.J., 2023. Loss of growth resilience towards the alpine shrubline. For. Ecol. Manage. 539, 121013. https://doi.org/10.1016/j.foreco.2023.121013.
Lu, X., Liang, E., Camarero, J.J., Ellison, A.M., 2021. An unusually high shrubline on the Tibetan Plateau. Ecology 102 (6), 1–4. https://www.jstor.org/stable/27070603.
Lu, X., Huang, R., Wang, Y., Zhang, B., Zhu, H., Camarero, J.J., Liang, E., 2020. Spring hydroclimate reconstruction on the south-central Tibetan plateau inferred from Juniperus pingii var. wilsonii shrub rings since 1605. Geophys. Res. Lett. 47 (12), e2020GL087707. https://doi.org/10.1029/2020GL087707.
Lu, X., Liang, E., Wang, Y., Babst, F., Leavitt, S.W., Julio Camarero, J., 2019. Past the climate optimum: Recruitment is declining at the world's highest juniper shrublines on the Tibetan Plateau. Ecology 100 (2), e02557. https://doi.org/10.1002/ecy.2557.
Luo, H., Wu, J., 2022. An assessment of the suitability of Sentinel-2 data for identifying burn severity in areas of low vegetation. J. Indian Soc. Remote Sens. 50 (6), 1135–1144. https://doi.org/10.1007/s12524-022-01518-7.
Macias-Fauria, M., Johnson, E.A., 2013. Warming-induced upslope advance of subalpine forest is severely limited by geomorphic processes. Proc. Natl. Acad. Sci. 110 (20), 8117–8122. https://doi.org/10.1073/pnas.1221278110.
Malapane, C., Dube, T., Dalu, T., 2024. Assessing the dynamics of land use and land cover change in semi-arid savannah: a focus on woody plant encroachment utilising historical satellite data. Afr. J. Ecol. 62 (3), e13300. https://doi.org/10.1111/aje.13300.
Minh, N.Q., Huong, N.T.T., Khanh, P.Q., Hien, L.P., Bui, D.T., 2024. Impacts of resampling and downscaling digital elevation model and its morphometric factors: a comparison of hopfield neural network, bilinear, bicubic, and kriging interpolations. Remote Sens. (Basel) 16 (5), 819. https://doi.org/10.3390/rs16050819.
Minowa, Y., 2008. Verification for generalizability and accuracy of a thinning-trees selection model with the ensemble learning algorithm and the cross-validation method. J. For. Res. 13 (5), 275–285. https://doi.org/10.1007/s10310-008-0084-6.
NASA JPL, 2020. NASADEM Merged DEM Global 1 arc second V001. NASA EOSDIS Land Processes Distributed Active Archive Center. Accessed 2025-03-31 from https://doi.org/10.5067/MEaSUREs/NASADEM/NASADEM_HGT.001.
Onačillová, K., Gallay, M., Paluba, D., Péliová, A., Tokarčík, O., Laubertová, D., 2022. Combining Landsat 8 and Sentinel-2 data in Google Earth Engine to derive higher resolution land surface temperature maps in urban environment. Remote Sens. (Basel) 14 (16), 4076. https://doi.org/10.3390/rs14164076.
Ostrowski, J.G., Menyhárt, J., 2020. Statistical analysis of machinery variance by python. Acta Polytech. Hung. 17 (5), 151–168. https://doi.org/10.12700/APH.17.5.2020.5.8.
Paulsen, J., Körner, C., 2014. A climate-based model to predict potential treeline position around the globe. Alp. Bot. 124 (1), 1–12. https://doi.org/10.1007/s00035-014-0124-0.
Peng, S., 2019. 1-km monthly mean temperature dataset for china (1901-2022). National Tibetan Plateau / Third Pole Environment Data Center. https://doi.org/10.5194/essd-11-1931-2019.
Pereira, S.C., Lopes, C., Pedro Pedroso, J., 2022. Mapping cashew orchards in cantanhez national park (guinea-bissau). Remote Sens. Appl.: Soc. Environ. 26, 100746. https://doi.org/10.1016/j.rsase.2022.100746.
Poggio, L., de Sousa, L.M., Batjes, N.H., Heuvelink, G.B.M., Kempen, B., Ribeiro, E., Rossiter, D., 2021. SoilGrids 2.0: Producing soil information for the globe with quantified spatial uncertainty. Soil 7 (1), 217–240. https://doi.org/10.5194/soil-7-217-2021.
Rösch, M., Sonnenschein, R., Buchelt, S., Ullmann, T., 2022. 2022, Comparing PlanetScope and Sentinel-2 Imagery for Mapping Mountain Pines in the Sarntal Alps Italy. Remote Sens 14, 3190. https://doi.org/10.3390/rs14133190.
Seastedt, T.R., Oldfather, M.F., 2021. Climate change, ecosystem processes and biological diversity responses in high elevation communities. Climate 9 (5), 5. https://doi.org/10.3390/cli9050087.
Sedgwick, P., 2012. Pearson's correlation coefficient. BMJ 345, e4483. https://doi.org/10.1136/bmj.e4483.
Shangguan, W., Li, Q., Shi, G., 2022. A 1 km daily soil moisture dataset over China based on in-situ measurement (2000-2022). National Tibetan Plateau / Third Pole Environment Data Center. https://doi.org/10.11888/Terre.tpdc.272415.
Shangguan, Z., Jing, X., Wang, H., Liu, H., Gu, H., He, J.-S., 2024. Plant biodiversity responds more strongly to climate warming and anthropogenic activities than microbial biodiversity in the qinghai–tibetan alpine grasslands. J. Ecol. 112 (1), 110–125. https://doi.org/10.1111/1365-2745.14222.
Smith, W.K., Germino, M.J., Johnson, D.M., Reinhardt, K., 2009. The altitude of alpine treeline: a bellwether of climate change effects. Bot. Rev. 75 (2), 163–190. https://doi.org/10.1007/s12229-009-9030-3.
Stueve, K.M., Cerney, D.L., Rochefort, R.M., Kurth, L.L., 2009. Post-fire tree establishment patterns at the alpine treeline ecotone: Mount Rainier National Park, Washington, USA. Journal of vegetation science 20 (1), 107–120. https://doi.org/10.1111/j.1654-1103.2009.05437.x.
Tchebakova, N.M., Parfenova, E., Soja, A.J., 2009. The effects of climate, permafrost and fire on vegetation change in siberia in a changing climate. Environ. Res. Lett. 4 (4), 45013. https://doi.org/10.1088/1748-9326/4/4/045013.
Torres, Y.A., Ithurrart, L.S., Ambrosino, M.L., Brendel, A.S., Blázquez, F.R., Armando, L. V., Pezzola, A., 2024. Shrub encroachment in semi-arid rangelands of southwestern buenos aires, argentina does not affect plant diversity and composition. J. Arid Environ. 222, 105140. https://doi.org/10.1016/j.jaridenv.2024.105140.
Xu, B., Li, J., Liu, Y., Zhang, T., Luo, Z., Pei, X., 2024. Disentangling the response of vegetation dynamics to natural and anthropogenic drivers over the Qinghai-Tibet Plateau using dimensionality reduction and structural equation model. For. Ecol. Manage. 554, 121677. https://doi.org/10.1016/j.foreco.2023.121677.
Van Staden, P.J., Bredenkamp, G.J., Bezuidenhout, H., Brown, L.R., 2021. A reclassification and description of the Waterberg Mountain vegetation of the Marakele National Park, Limpopo province, South Africa. https://repository.up.ac.za/handle/2263/87183.
Wang, M., Mao, D., Wang, Y., Xiao, X., Xiang, H., Feng, K., Wang, Z., 2023. Wetland mapping in East Asia by two-stage object-based Random Forest and hierarchical decision tree algorithms on Sentinel-1/2 images. Remote Sens. Environ. 297, 113793. https://doi.org/10.1016/j.rse.2023.113793.
Wang, Y., Liang, E., Lu, X., Camarero, J.J., Babst, F., Shen, M., Peñuelas, J., 2021. Warming-induced shrubline advance stalled by moisture limitation on the Tibetan Plateau. Ecography 44 (11), 1631–1641. https://doi.org/10.1111/ecog.05845.
Wei, C., Karger, D.N., Wilson, A.M., 2020. Spatial detection of alpine treeline ecotones in the Western United States. Remote Sens. Environ. 240, 111672. https://doi.org/10.1016/j.rse.2020.111672.
Wu, Z., Wang, W., Zhu, W., Zhang, P., Chang, R., Wang, G., 2024. Shrub ecosystem structure in response to anthropogenic climate change: a global synthesis. Sci. Total Environ. 953, 176202. https://doi.org/10.1016/j.scitotenv.2024.176202.
Yang, J., Weisberg, P.J., Bristow, N.A., 2012. Landsat remote sensing approaches for monitoring long-term tree cover dynamics in semi-arid woodlands: Comparison of vegetation indices and spectral mixture analysis. Remote Sens. Environ. 119, 62–71. https://doi.org/10.1016/j.rse.2011.12.004.
Zhao, Q., Hao, X., Wang, J., Luo, S., Shao, D., Li, H., Zhao, H., 2022. Snow cover phenology change and response to climate in China during 2000–2020. Remote Sens. (Basel) 14 (16), 3936. https://doi.org/10.3390/rs14163936.
Zhang, L., Yan, E.R., Wei, H.X., Liu, X.S., Shen, W., 2014. Leaf nitrogen resorption proficiency of seven shrubs across timberline ecotones in the Sergymla Mountains, Southeast Xizang, China. Chinese J. Plant Ecol. 38 (12), 1325. https://doi.org/10.3724/SP.J.1258.2014.00127.
Zhang, L., Li, X., Zheng, D., Zhang, K., Ma, Q., Zhao, Y., Ge, Y., 2021. Merging multiple satellite-based precipitation products and gauge observations using a novel double machine learning approach. J. Hydrol. 594, 125969. https://doi.org/10.1016/j.jhydrol.2021.125969.
Zhang, X., Liu, J., Zeng, J., et al., 2024. Impact of drought-induced forest mortality on terrestrial carbon cycle from remote sensing perspective. Innovation Geosci. 2 (1), 100057. https://doi.org/10.59717/j.xinn-geo.2024.100057.
Zou, L., Tian, F., Liang, T., Eklundh, L., Tong, X., Tagesson, T., Fensholt, R., 2023. Assessing the upper elevational limits of vegetation growth in global high-mountains. Remote Sens. Environ. 286, 113423. https://doi.org/10.1016/j.rse.2022.113423.